IEEE Access
Multidisciplinary ⋮ Rapid Review ⋮ Open Access Journal

Received January 4, 2021, accepted January 18, 2021, date of publication January 26, 2021, date of current version February 12, 2021.

Digital Object Identifier 10.1109/ACCESS.2021.3054591

Novel Selective Feeding Scheme Integrated With SPDT Switches for a Reconfigurable Bandpass-to-Bandstop Filter

SALMAN ARAIN[1], (Member, IEEE), PHOTOS VRYONIDES[2], (Member, IEEE), KASHIF NISAR[3,4], (Senior Member, IEEE), ABDUL QUDDIOUS[5], (Member, IEEE), AND SYMEON NIKOLAOU[2], (Member, IEEE)

[1]Electrical Engineering Department, NFC-Institute of Engineering & Fertilizer Research, Faisalabad 38000, Pakistan
[2]Frederick Research Center (FRC), Frederick University, 1036 Nicosia, Cyprus
[3]Faculty of Computing and Informatics, University Malaysia Sabah, Kota Kinabalu 88400, Malaysia
[4]Department of Computer Science and Engineering, Hanyang University, Seoul 04763, South Korea
[5]KIOS Research and Innovation Center of Excellence, University of Cyprus, 2109 Nicosia, Cyprus

Corresponding author: Kashif Nisar (kashif@ums.edu.my)

This work was supported in part by the APC funded by PPPI, University Malaysia Sabah, and in part by the European Regional Development Fund and the Republic of Cyprus through the Research and Innovation Foundation under Project EXCELLENCE/1216/376 (SWITCH) and Project EXCELLENCE/0918/0365 (ICARUS).

ABSTRACT This paper demonstrates a new technique for designing high performance reconfigurable bandpass-to-bandstop filters by employing a ring resonator and a selective feeding scheme integrated with single-pole double-throw switches (SPDT). The transformation from bandpass-to-bandstop mode and vice-versa is achieved by connecting or disconnecting two $\lambda_g/4$ open-circuited stubs on the ring using PIN diodes. SPDT switches are employed for electronic switching between two different feeding line sections. In the bandpass state the resonator presents two transmission zeros near the edges of the passband and four attenuation poles inside the passband, enhancing the filter's performance, thus achieving excellent sharp rejection with high roll-off-rate (ROR_{20dB}). On the other hand, high stopband rejection with wide bandwidth, good return loss and good skirt-band attenuation rates are achieved in the bandstop state. Even- and odd-mode analysis is adopted and closed-form expressions are derived to describe the filter's behaviour. To verify the validity of the proposed design, a prototype filter was fabricated and measured. In measurement, a 65% 3-dB bandwidth bandpass filter (BPF) with an insertion loss of 0.86 dB was switched to a 70% 20-dB bandwidth bandstop filter (BSF) with more than 40 dB stopband rejection.

INDEX TERMS Bandpass filter (BPF), bandstop filter (BSF), PIN diodes, ring resonator, single-pole-double-throw (SPDT).

I. INTRODUCTION

With the recent rise in the demand for electromagnetic spectrum due to the increasing spread of microwave and wireless system applications, reconfigurable microwave filters are anticipated to facilitate the growth of modern multi-functional transceivers operating in an immensely vigorous interference environment, without the need for complex and large in size filter banks. In this environment bandstop filters (BSF) [1]–[9] are the key components for elimination of high power-agile interferers close to the desired signal, whereas bandpass filters (BPF) are chosen for the selection of the desired RF signals [10]–[13]. Therefore recently, reconfigurable filters have become an essential component in wireless systems and have attracted a lot of attention. Even though tunable single and multiband filtering components have been proposed [14]–[24] with a number of advantages, they usually serve a single purpose (either tunable BPF or tunable BSF). Few researchers [25]–[32] have presented fully reconfigurable filtering circuits exhibiting BPF-to-BSF switching capability. The filter in [25] demonstrates a switching capability between narrowband filter functions, either a Butterworth bandpass response or a Chebyshev bandstop response by switching the feeding structure using the same

The associate editor coordinating the review of this manuscript and approving it for publication was Vincenzo Conti.

set of coupled resonators. In [26], filter reconfigurability from bandstop to bandpass response is achieved by implementing MEMS switches based on a new

bandstop filter topology using inter-resonator coupling structures. A tunable filter exhibiting BPF-to-BSF transition as well as bandwidth control achieved by adjusting the coupling coefficients of the resonator was shown in [27] whereas in [28] the BPF-to-BSF response as well as reconfigurable 2- and 4- pole responses is achieved using silicon varactor diodes and RF MEMS switches. The filter in [29] utilizes a varactor-loaded closed-ring resonator to control the bandpass and bandstop characteristics by tuning the varactor's bias voltage. A reconfigurable BPF-to-BSF has been proposed in [30] based on the square ring resonator with stepped impedance open-circuited stubs in the same frequency band, however mathematical analysis and design formulas were not provided. Recently, a compact tunable BPF-to-BSF filter is presented in [31] by employing PIN diodes for switching between states and varactors for centre frequency tuning. Finally in [32], a reconfigurable BPF-to-BSF was proposed based on frequency evanescent mode cavity resonators, integrated in microstrip technology.

RF switches are also very important in time division duplex wireless communication systems. Integrating filters and switches in a single circuit has the advantage of decreasing the cost as well as the circuit size and complexity. Lately a number of single-pole double throw (SPDT) reconfigurable BPFs are suggested [33]–[38]. In [33] a SPDT switchable BPF which is based on a capacitively multicoupled line using electromagnetic coupling to replace the quarter-wavelength line is demonstrated. In [34] a new method is proposed to integrate a SPDT switch and a quarter-wavelength BPF. To achieve sharp passband selectivity SPDT switch with a BPF using the shorted stepped-impedance resonator technique can be adopted as in [35]. In [36] a new SPDT switch together with a switchable transmission line stub resonators are implemented to achieve a selectable multiband isolation whereas in [37] a new method using PIN diodes and SPDT switch is proposed to switch between two channels of a tunable diplexer. Lastly, a quasi-lumped element filter integrated with SPDT switch with low insertion loss and sharp passband selectivity is presented in [38].

In this paper, a novel reconfigurable BPF-to-BSF prototype is proposed based on the square ring resonator and the transmission-line method where the feeding lines are integrated with SPDT switches to select different feeding lines for the bandpass and bandstop state in order to provide a wide upper stopband and excellent sharp skirt selectivity in the bandpass state and good passband return loss and stopband rejection while in bandstop state. The microstrip square ring resonator is chosen due to its compact size, low radiation loss and high Q- factor. The proposed design is simple, and low cost with sharp rejection and wideband bandwidth compared to the aforementioned proposed designs. Accurate formulas are derived and are employed to calculate the even- and odd-mode resonant frequencies and the frequency locations of the transmission zeros. Such reconfigurable BPF-to-BSF is a good candidate for frequency tunability in the cognitive radio systems, alternating transmission and reception schemes in highly congested environments, transceivers operating in strong interference environment, RF diplexers, and other filtering circuits having both BPF/BSF operational modes.

This manuscript is organized as follows: In the following section, the basic filter theory of the proposed ring resonator is analyzed. In section III, the hardwire cases for the design of the BPF and the BSF are presented whereas in section IV the SPDT switching capabilities for the enhancement of the performance of the reconfigurable filter are illustrated. The final section of the paper demonstrates the experimental results of the prototype reconfigurable filter followed by the conclusions.

II. THEORY AND DESIGN EQUATIONS FOR FILTERS

The initial proposed schematics of the ring resonator filters (BPF, BSF) are shown in Fig. 1(a) to (d). Both filtering states utilize a square ring resonator which is an unloaded ring (BSF) or loaded with a pair of $\lambda_g/4$ open-circuited (BPF) stubs connected at the center of the right and top sides of the ring [39]. The input and output ports are selected at the two orthogonal positions, i.e. at the center of the bottom and left sides of the ring and are directly connected to the ring. The ring perimeter is one wavelength long with characteristic impedance Z_1. In the most general description, the electrical length of the side of the ring is θ_1, while the open-circuited stubs have electrical length θ_2 and characteristic impedance Z_2. Simulated reflection and transmission responses for the BSF and BPF are presented in Fig. 1(e) and (f) respectively. As can be seen the bandstop response suffers from poor out-of-band return loss and poor passband insertion loss, whereas poor rejection at the stopband is also noted for the bandpass response. Under weak coupling [40], [41] the plane of symmetry XX' shown in Fig. 2(a), can be considered as either a perfect magnetic or a perfect electric wall respectively. The equivalent even/odd mode circuits of the ring resonator which are used to determine the resonant frequencies of the filters are shown in Figs. 2(b) and 2(c) respectively.

Fig. 2(d) shows the comparison of calculated S_{21} (magnitude in dB) under weak coupling when $\theta_2 = \theta_1 = \pi/2$, when the ring is loaded with open- and short- circuited quarter wavelength stubs respectively. Under weak coupling, Fig. 2(d) depicts the even/odd mode resonant frequencies. We first consider the case shown in Fig. 1(b) where the ring is loaded with open-circuited stubs (BPF). From Fig. 2(d) it can be seen that there are four transmission poles in the desired frequency band and two transmission zeros located at the upper and lower cut-off frequencies, achieving sharp selectivity. As the coupling is increased i.e. strong coupling, a wide passband is formed from 1.8- 3.1 GHz with a simulated fractional bandwidth of 63%. As shown in [42] with strong coupling elements at the two excited ports, these

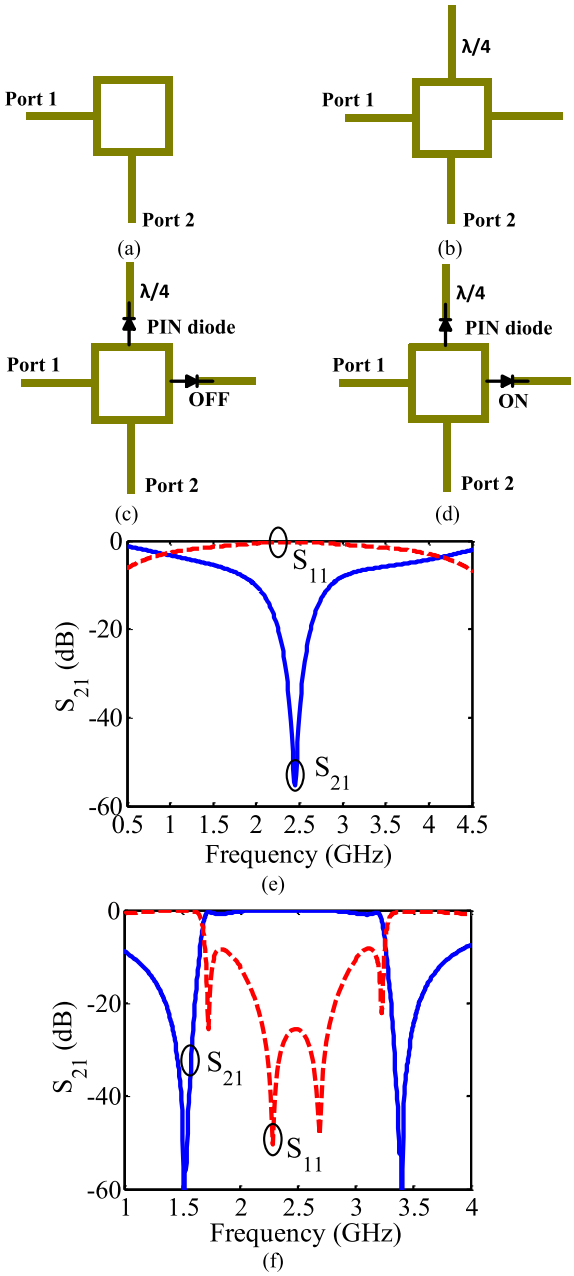

FIGURE 1. Hardwire and reconfigurable designs configuration. (a) unloaded ring resonator, (b) loaded ring resonator with tuning stubs, (c) switchable filter design for BSF, (d) switchable filter design for BPF, (e) BSF response, (f) BPF response.

four poles are combined to realize a wide passband. From ring resonator theory, it can be said that the ring resonates when its input admittance is zero [40]. Thus, the resonant conditions are displayed as,

$$Y^{even} = Y^{even,1} + Y^{even,2} = 0 \quad (1)$$

$$Y^{odd} = Y^{odd,1} + Y^{odd,2} = 0 \quad (2)$$

Superscripts 1 and 2 represent the upper and lower arm input admittance respectively as defined in Fig. 2.

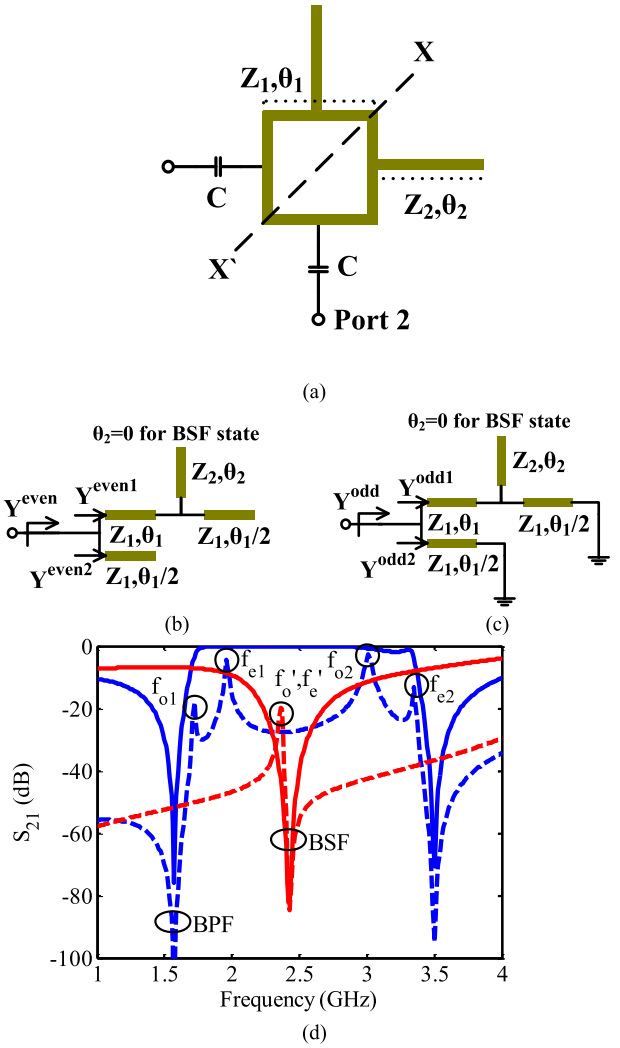

FIGURE 2. Even and odd mode analysis. (a) initial design with weak coupling, (b) even-mode analysis circuit, (c) odd-mode analysis circuit, (d) weak/strong coupling analysis for BPF and BSF states.

A. EVEN-ODD MODE ANALYSIS AND TRANSMISSION ZEROS WITH ARBITRARY LONG OPEN-CIRCUITED STUBS

Here, a thorough analysis of the square ring resonator loaded with open-circuited stub is presented, by using the even-odd mode method for computing the resonance $y^{even} = 0$, frequencies and the transmission zeros (TZs). The even-mode equivalent circuit when a magnetic wall is applied on the plane of symmetry XX′ of the ring resonator is displayed in Fig. 2(b). The analysis is simplified by neglecting all the effects generated by transmission line discontinuities that are incorporated in the resonator shown in Fig. 2(a). The normalized even-mode input admittance $Y^{even,1}$ and $Y^{even,2}$ of the upper and lower arms, respectively are expressed by,

$$Y^{even,1} = j\frac{-p^3 - Kqp^2 + 3p + Kq}{-3p^2 - 2Kqp + 1} \quad (3a)$$

$$Y^{even,2} = jp \quad (3b)$$

Hence, applying the condition for resonance (1), the even-mode resonance occurs when

$$Y^{even} = -j\frac{4p^3 + 3Kqp^2 - 4p - Kq}{-3p^2 - 2Kqp + 1} = 0 \quad (3c)$$

where $K = Z_1/Z_2$, $p = \tan(\theta_1/2)$, and $q = \tan\theta_2$.

The odd-mode analysis is similar to the even mode. Fig. 2(c) displays the equivalent circuit representation of half the ring resonator when an electric wall is applied along XX′. The normalized odd-mode input admittance $Y^{odd,1}$ and $Y^{odd,2}$ of the upper and lower arms, respectively, have been derived as,

$$Y^{odd,1} = -j\frac{Kqp^3 - 3p^2 - Kqp + 1}{-p^3 - 2Kqp^2 + 3p} \quad (4a)$$

$$Y^{odd,2} = 1/jp \quad (4b)$$

Hence, the odd-mode resonance condition (2) can be obtained by,

$$Y^{odd} = j\frac{Kqp^3 - 4p^2 - 3Kqp + 4}{p^3 + 2Kqp^2 - 3p} = 0 \quad (4c)$$

If the ring is assumed to be lossless, the frequencies f_{z1} and f_{z2} at which the transmission zeros are located can be obtained as in [40], by solving,

$$Y^{odd} - Y^{even} = 0 \quad (5)$$

By substituting (3c) and (4c) into (5), the following polynomial equation can be obtained,

$$p^6 + 2Kqp^5 + (K^2q^2 - 1)p^4 + (K^2q^2 - 1)p^2 - 2Kqp + 1 = 0 \quad (6)$$

The polynomial equation has variables p and with q being the impedance ratio. In (6) the parameter q needs to be set so that with a given impedance ratio, and taking only the real positive roots of p, the corresponding electrical lengths (θ_2), where a transmission zero occurs can be calculated. The TZs frequencies can then be calculated by the following equation,

$$f_z = \frac{4\theta_1 c}{2\pi\lambda_g\sqrt{\varepsilon_{eff}}} \quad (7)$$

where, c is the speed of light in free space, λ_g is the guided wave length, and ε_{eff} is the effective dielectric constant. Similarly, the transmission pole (TP) frequencies of the ring filter may be calculated by solving,

$$Y^{odd}Y^{even} = 1 \quad (8)$$

By substituting (3c) and (4c) into (8), the following equation can be obtained,

$$4Kqp^6 + (3K^2q^2 - 13)p^5 - 20Kqp^4 + (6K^2q^2 + 22)p^3 + (3K^2q^2 + 20)p^2 - 13p - 4Kq = 0 \quad (9)$$

So as in (6) a set of solutions of electrical lengths (θ_2) where a transmission pole (TP) occurs can then be calculated. Based on the above discussion, the analysis method for the ring resonator filter with quarter-wavelength open-circuited stubs introducing two TZs fed by direct-connected feeding lines is presented in the following section.

B. RING WITH QUARTER-WAVELENGTH OPEN-CIRCUITED STUBS

Fig. 1(b) shows the schematic of a wideband ring resonator bandpass filter loaded with two identical quarter-wavelength long ($\theta_1 = \theta_2$) open-circuited stubs [43]. The total periphery of the ring is equal to one guided wavelength having characteristic impedance Z_1, whereas Z_2 is the characteristic impedance of the open-circuited stubs. Z_1 is also the characteristic impedance of the input and output feeding lines. By substituting $q = tan(\theta_1) = 2p/(1 - p^2)$ in (9) the following polynomial equation for obtaining the transmission zeros is derived,

$$p^{10} - (4K + 3)p^8 + (4K^2 + 4K + 2)p^6 + (4K^2 + 4K + 2)p^4 - (4K + 3)p^2 + 1 = 0 \quad (10)$$

Similarly doing the same substitution for q in equations (3c) and (4c) and by finding the positive roots of p in equations (3c) and (4c) the even/odd resonant frequencies can be predicted in an explicit manner. Equations (3c) and (4c) reveal that two even and two odd mode frequencies are present. In addition, by finding the roots of p in (10), the locations of the transmission zeros that are introduced by the $\lambda_g/4$ open-circuited stubs, in the real frequency plane can be predicted. Fig. 3(a) illustrates the TZs and transmission poles in the complex plane under $K = 1$. As it can be seen the $\lambda_g/4$ open-circuited stubs excite a pair of TZs and three transmission poles in the real frequency line. Table 1 includes the calculated and simulated positions of the even/odd resonances and the transmission zeros. Inspecting these results, it can be said that the simulated results are in very good agreement with the numerically calculated results proving the validity and accuracy of the equations derived above. Equation (10) reveals that two transmission zeros frequencies; f_{z1} and f_{z2} are located at the left and right of the first (f_{o1}) and fourth (f_{e2}) resonance respectively. Thus, the approximate bandwidth can be estimated by investigating two transmission zeros and two resonant frequencies in Fig. 3(b) and Fig. 4(a). The positions of these transmission zeros are solely determined by the impedance ratio K. Fig. 3(b) shows the first two normalized, transmission zeros with respect to the fundamental frequency f_0, transmission zero frequencies of the ring resonator against the length ratio t = θ_2/θ_1 under the impedance ratio $K = 0.5$, 1 and 2. From this figure, it is observed that both of the transmissions zeros are shifted towards lower frequencies and also their frequency separation

TABLE 1. Comparison between calculated and simulated resonant frequencies (Units: GHZ).

Frequencies	Calculated	Simulated
f_{e1}	1.88	1.92
f_{o1}	1.60	1.63
f_{e2}	3.20	3.24
f_{o2}	2.92	2.92
f_{z1}	1.46	1.52
f_{z2}	3.34	3.42

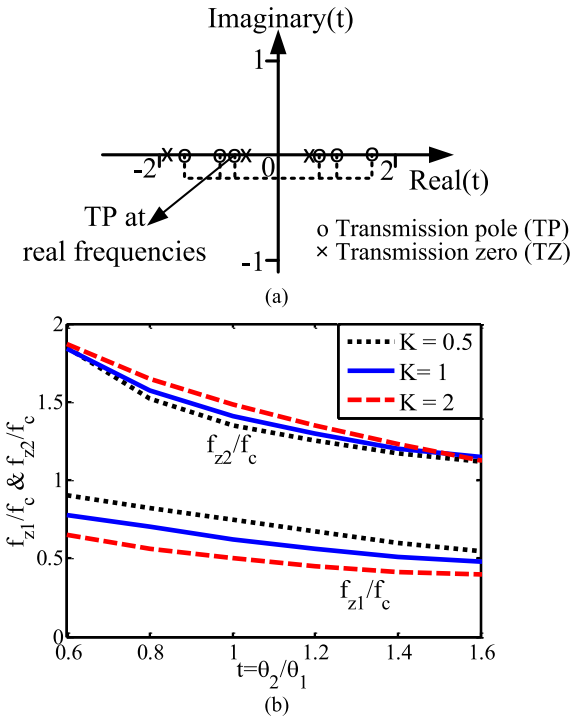

FIGURE 3. (a) Locations of TZ and poles of the ring loaded with $\lambda_g/4$ open-circuited stubs, (b) normalized TZs (f_{z1}, f_{z2}) versus length ratio 't' under different values of K.

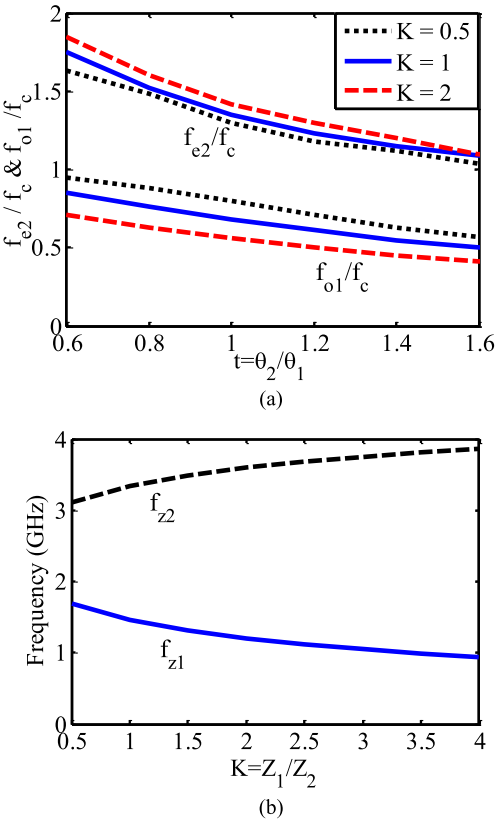

FIGURE 4. (a) Resonant frequencies (even-mode: f_{e2}, odd-mode: f_{o1} versus length ratio 't' under different values of K, (b) locations of the TZ against K at t = 1.

uniformly decreases with increase of the θ_2/θ_1 ratio for all values of K. Based on the analysis discussed in section A, all the even and odd mode frequencies can be solved by finding the roots of (3c) and (4c) respectively. Fig. 4(a) plots the first odd-mode (f_{o1}) and the second even-mode (f_{e2}) resonant frequencies normalized by the center frequency (f_0) versus the length ratio of t = θ_2/θ_1 under different values of the impedance ratio K. It can be seen that the frequency separation of f_{e2}-f_{o1} is smaller for lower values of K and vice versa and also f_{o1} and f_{e2} seem to progressively move to lower frequencies as the length ratio θ_2/θ_1 increases to 1.5. Since f_0 is considered to be the desired center frequency, then $f_{e2}-f_{o1}$ at a specific (θ_2/θ_1) ratio is considered to be approximately the passband bandwidth. This also shows that the bandwidth of the filter can be decreased by approximately 30% if a lower value of K is used. Fig. 4(b) displays the positions of the transmission zeros against the impedance ratio K under the length ratio t = 1. It can be seen that as K is changed from 0.5 to 4 the frequency separation between these two transmissions zeros increases. The calculated and simulated resonant and transmission zero frequencies are shown in Table 1 for the condition of K = 1 and are in good agreement with each other providing solid proof that the derived equation (10) is very accurate.

Fig. 5 plots the transmission pole frequencies (f_{o1}, f_{e1}, f_{o2} and f_{e2}) and the transmission zero frequencies (f_{z1}, f_{z2}) against the length ratio t = θ_2/θ_1 under the condition of $K = 1$. From Fig. 5(a), it can be found that all four transmission pole frequencies decrease simultaneously as the length ratio (t) increases. In addition, the frequency separation of the first (f_{o1}) resonance and the first transmission zero frequency f_{z1} remains almost unchanged. The same is valid for the frequency separation of the fourth resonance (f_{e2}) and the second transmission zero f_{z2}. It can also be seen that for t = 1 all resonances are uniformly located in the passband making the filter a quadruple-mode one. Based on the above analysis, by applying direct- connected feeding lines to the presented ring resonator as shown in Fig. 1(b), the wideband BPF can be realized. In the following section the analysis for the unloaded ring resonator fed by direct-connected feeding lines is presented.

C. ANALYSIS OF UNLOADED RING RESONATOR

The unloaded ring resonator which is fed by direct-connected feeding lines is shown in Fig. 1(a) exhibits a bandstop characteristic. The analysis of this ring is provided in [44]. However, formulas to determine the resonant frequencies and the locations of the transmission zeros are not provided. By using the same analysis as in subsections *A and B,* the following normalized even-odd input admittances have been derived for the BSF of Fig. 2(b) and Fig. 2(c).

$$Y^{even} = j\frac{-4p^3 + 4p}{-3p^2 + 1} = 0 \tag{11}$$

$$Y^{odd} = -j\frac{4p^2 - 4}{p^3 - 3p} = 0 \tag{12}$$

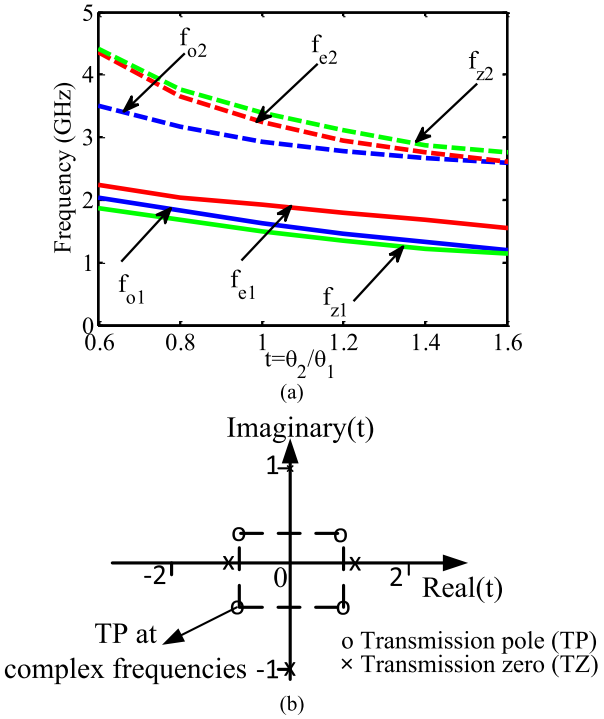

FIGURE 5. (a) TZs and TPs frequencies versus length ratio 't', (b) locations of TZs and poles for the unloaded ring filter.

Furthermore, the following formulas for determining the transmission zeros and poles are also derived in (9) and (10) respectively.

$$p^6 - p^4 - p^2 + 1 = 0 \tag{13}$$

$$13p^4 - 22p^2 + 13 = 0 \tag{14}$$

The solutions of (13) and (14) are shown in Fig. 5(b). As it can be seen the unloaded ring resonator filter generates only a single TZ in the real frequency plane as well as two complex conjugate transmission pole pairs. Roots that are complex do not have any influence on the filter's response due to the complex resonant frequency [45]. A comparison between all the resonances (even/odd and TZs) calculated by the formulas and those computed by the simulator are shown in Table 1 and again are in very good agreement.

Based on the above discussion, it is clear that the addition of quarter-wavelength open-circuited stubs on the ring generates two transmission zeros, the locations of which are strongly dependent on the value of impedance ratio K. The higher the value of K, the wider the bandwidth of the filter. The performance of a ring without any stubs connected to it was also analyzed. An unloaded ring also exhibits bandstop characteristics generating a single transmission zero whose location is independent of K. Furthermore, an unloaded ring introduces two pairs of transmission poles located in the complex plane without having any influence of the filter's response. However, both bandstop and bandpass responses suffer from poor electrical performance in terms of out-of-band return loss and passband insertion loss in the bandstop case and poor stopband performance in the bandpass case. In the following sections a novel technique to improve the performances of both states is described in detail.

III. FILTER DESIGN FOR BPF AND BSF

According to the detailed mathematical analysis given in Section II, a BPF and a BSF are designed by employing a pair of $\lambda_g/4$ parallel coupled lines (for BPF) and a pair of stepped impedance transmission lines parallel to a pair of $\lambda_g/4$ open stub (for BSF) as feeding lines. Fig. 6(a) shows the layout of the BPF design which is driven by two $\lambda_g/4$ parallel coupled lines (PCLs) which are connected perpendicularly on the ring sides. The ABCD matrix of the parallel coupled lines is depicted in (15).

$$\begin{bmatrix} A & B \\ C & D \end{bmatrix} = \begin{pmatrix} \dfrac{Z_e + Z_o}{Z_e - Z_o}\cos\theta_c & j\dfrac{(Z_e - Z_o)^2 - (Z_e + Z_o)^2\cos^2\theta_c}{2(Z_e - Z_o)\sin\theta_c} \\ j\dfrac{2\sin\theta_c}{Z_e - Z_o} & \dfrac{Z_e + Z_o}{Z_e - Z_o}\cos\theta_c \end{pmatrix} \tag{15}$$

Y_{21} can be extracted by converting the ABCD matrix into Y matrix as given in (16),

$$Y_{21} = 2j\frac{(Z_e - Z_o)\sin\theta_c}{(Z_e - Z_o)^2 - (Z_e + Z_o)^2\cos^2\theta_c} \tag{16}$$

The solutions obtained by (16) when Y_{21} is set to zero correspond to $\theta = 0$ and π (0 and $2f_0$). The dimensions of the PCLs are optimized and adjusted based on the requirement to achieve a wide upper stopband.

The simulated comparison between the uniform transmission feeding lines (UTFL) and the PCLs are shown in Fig. 6(b). It is observed from Fig. 6(b) that by employing the PCLs as feeding lines two out-of-band transmission zeros are generated around DC and $2f_0$ which in turn suppress the unwanted harmonics thus achieving wide stopband and sharp rejection. The upper stopband rejection is greater than -25 dB for up to 6.3 GHz (2.62 f_0). In addition, with the proposed design, an improvement in the return loss within the passband is also clearly seen.

Fig. 7(a) illustrates the schematic layout of the BSF by utilizing a pair of stepped impedance transmission feeding lines (SITFL) that are parallel to a pair of open stubs whereas Fig 7(b) and Fig. 7(c) depict the corresponding even- and odd-mode equivalent circuit. Initially three feeding lines namely UTFL, stub loaded transmission feeding lines (SLTFL), and SITFL are analyzed and the simulated results are displayed in Fig. 7(d). By employing the even- and odd-mode analysis along the symmetry AA' the even and odd mode resonant conditions are derived in (17) and (18) respectively,

$$Y^{even} = \frac{-4p^8 + p^6(c) - p^4(b) + p^2(a) - K'}{-p^7(g) + p^5(f) - p^3(e) + p(d)} \tag{17}$$

$$Y^{odd} = \frac{K'p^8 - p^6(a) + p^4(b) - p^2(c) + 4}{-p^7(d) + p^5(f) - p^3(g) + p(h)} \tag{18}$$

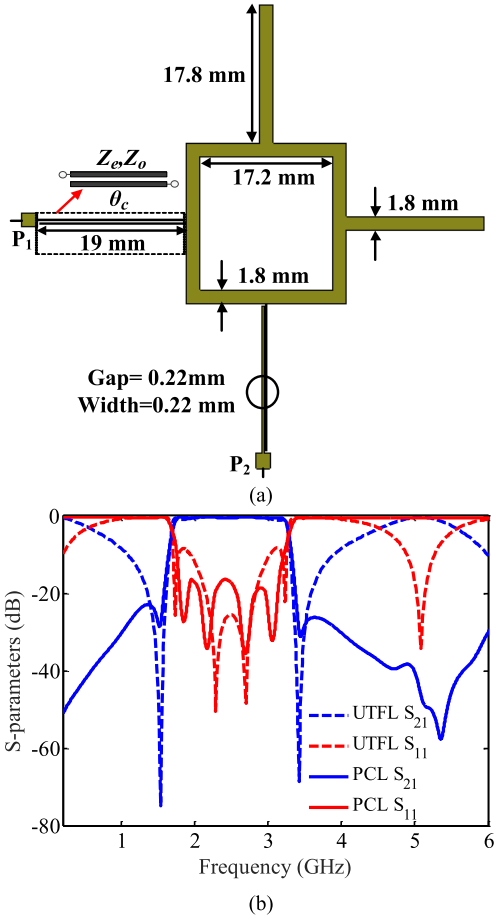

FIGURE 6. (a) Proposed design of improved BPF with parallel coupled feeding lines, (b) S-parameters comparison between uniform and parallel coupled feeding lines.

where,

$$a = 13K' + 2K + 6 \tag{19}$$
$$b = 23K' + 24K + 20 \tag{20}$$
$$c = 11K' + 22K + 18 \tag{21}$$
$$d = K' + 2K + 6 \tag{22}$$
$$e = 13K' + 24K + 20 \tag{23}$$
$$f = 23K' + 22K + 18 \tag{24}$$
$$g = 11K' + 4 \tag{25}$$

and the impedance ratios K and K' are

$$K = Z_1/Z_2 \tag{26}$$
$$K' = Z_1/Z_3 \tag{27}$$

The solutions of the even- and odd-mode resonances correspond to the six transmission poles as displayed in Fig. 9(b).

From Fig. 7(d), it is observed that with the addition of the open stubs, the 20-dB stopband bandwidth is increased and in addition extra transmission poles are generated in the passband region, however return loss is not greatly

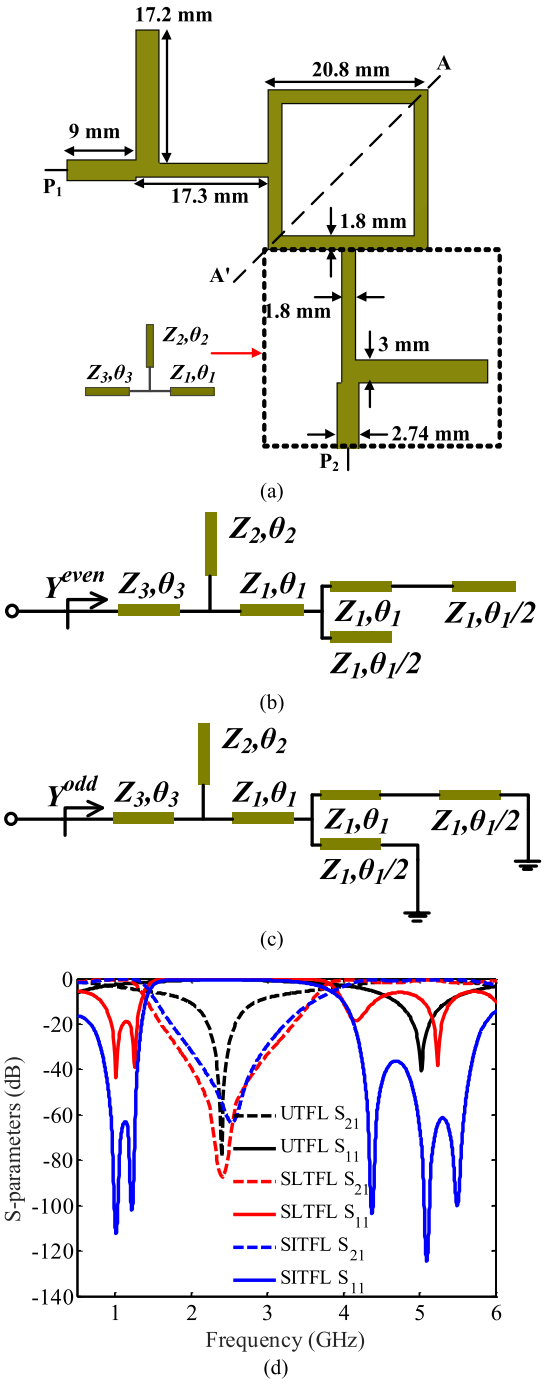

FIGURE 7. (a) Proposed design of improved BSF with SITFL, (b) even-mode equivalent circuit, (c) odd- mode equivalent circuit (d) S-parameters comparison between different feeding lines.

improved. With the addition of the SITFL, the 20-dB stopband bandwidth is increased more and the return loss is greatly improved in the passband region up to 5.6 GHz with return loss greater than 15 dB. The BSF also provides simulated stopband rejection of about 60 dB in the operating region. The following circuit parameters were used for BSF: $Z_1 = 50\ \Omega$, $\theta_1 = 90°$, $Z_2 = 35\ \Omega$, $\theta_2 = 90°$, $Z_3 = 38\ \Omega$, $\theta_3 = 45°$.

IV. IMPLEMENTATION OF SWITCHABLE BPF/BSF USING SELECTIVE FEEDING SCHEME

Fig. 8(a) and Fig. 8(b) show the geometry of the selective feeding scheme for the BSF and BPF case along with the dimensions and the required components. To achieve electronic switching, two SPDT RF switches (CEL's CG2415M6 pHEMT GaAs MMIC) [46] were used to switch between the BSF feeding line section and BPF feeding line section.

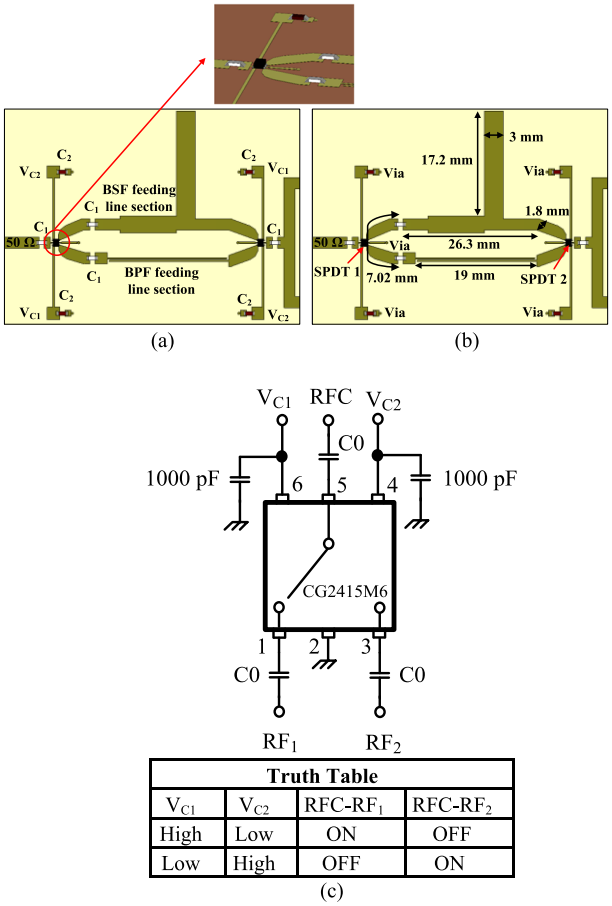

Truth Table			
V_{C1}	V_{C2}	RFC-RF_1	RFC-RF_2
High	Low	ON	OFF
Low	High	OFF	ON

FIGURE 8. (a) Design structure of the proposed reconfigurable feeding line sections for switching between BPF and BSF states along with SPDT switch IC and circuitry, (b) dimensions of the proposed reconfigurable feeding line sections, (c) evaluation circuit of SPDT IC along with its truth Table.

CEL's CG2415M6 is a bidirectional SPDT switch with all RF ports impedance 50 Ω and is specifically suitable for WLAN applications. For the biasing network, small square pads of 2 × 2 mm^2 are introduced to connect to DC lines via short DC bypass capacitors (C_2 = 1000pF). These capacitors were used as DC bypass to protect the DC power supply from the leakage of RF energy. Fig. 8(c) shows the circuit schematic with the associated voltage truth table. A DC blocking capacitor (C_1) of 8 pF is required at all RF ports to block the DC power from the RF signal path. CST Microwave Studio was used to design the filter. The manufacturer's S-parameter files for the SPDT switches and the library models for the capacitors were used in co-simulation environment with CST design studio in order to ensure an accurate simulation model for the implemented hardware. The SMA connectors were also included in the simulation model to improve the agreement between the simulated and the measurement results.

The used SPDT switch is available in a 6-pin lead-less mini mold package of size 1.5 × 1.1 × 0.55 mm^3. Fig. 8 shows the mounting pad layout for the 6-pin IC that was also considered in the full wave simulations. To switch between the BSF feeding section and the BPF feeding line section, control voltages on both V_{C1} and V_{C2} terminals (Fig. 8(c)) are needed.

Based on the above discussion, a fully switchable BPF/BSF with reconfigurable feeding line sections was fabricated and measured. The reconfigurable BPF/BSF was fabricated on a Roger's RT Duroid 4003C substrate with ε_r = 3.55 and tanδ = 0.0027 with substrate thickness of 0.813 mm, and conductor thickness of 0.035 mm. The proposed design was implemented by standard PCB milling machine (LPKF ProtoMatH100). The S-parameters measurement was conducted using an Agilent E8363B Vector Network Analyzer (VNA). A 3V DC voltage source was applied around the patches connected with RF chokes of 82 nH to bias the PIN diodes (Skyworks SMP1345- 079LF) with a series resistor across the square ring.

In order to implement the electronic switching the appropriate feeding line section must be selected. BPF, requires V_{C1} high control voltage (+3V) and V_{C2} low control voltage (0V) for SPDT1 and the opposite for SPDT2. Evidently for BSF requires the opposite biasing conditions for the two RF switches.

V. MEASUREMENTS AND RESULTS

A prototype of the reconfigurable filter structure described in sections III and IV with a centre frequency of 2.4 GHz was fabricated to validate the simulated results. The simulated and measured results are displayed in Fig. 9(a) and Fig. 9(b) together with a photograph of the prototype in Fig. 9(c). First, the PIN diodes were turned on to have a bandpass response and at the same time the SPDT switches were switched to the BPF feeding line sections to attain a wide upper stopband.

Fig. 9(b) presents the simulated and measured results for the reconfigurable filter in the bandstop mode. When the BPF feeding line sections are ON, the BPF provides a 3-dB fractional bandwidth of 65 % having return loss greater than 15 dB with insertion loss less than 0.86 dB. The stopband rejection range for the BPF state is 2.62f_0. To analyze the measured steepness of the transition band, the roll- off rate ($ROR_{20\ dB}$) is defined as,

$$ROR_{20dB} = \frac{|X_{20dB} - X_{3dB}|}{|f_{20dB} - f_{3dB}|} \tag{28}$$

where X_{3dB} and $X_{20\ dB}$ are the 3- and 20-dB attenuation points respectively, and $f_{3\ dB}$ and $f_{20\ dB}$ are the 3- and 20-dB stopband frequency points respectively. The $ROR_{20\ dB}$ of the proposed BPF transitions bands are calculated as

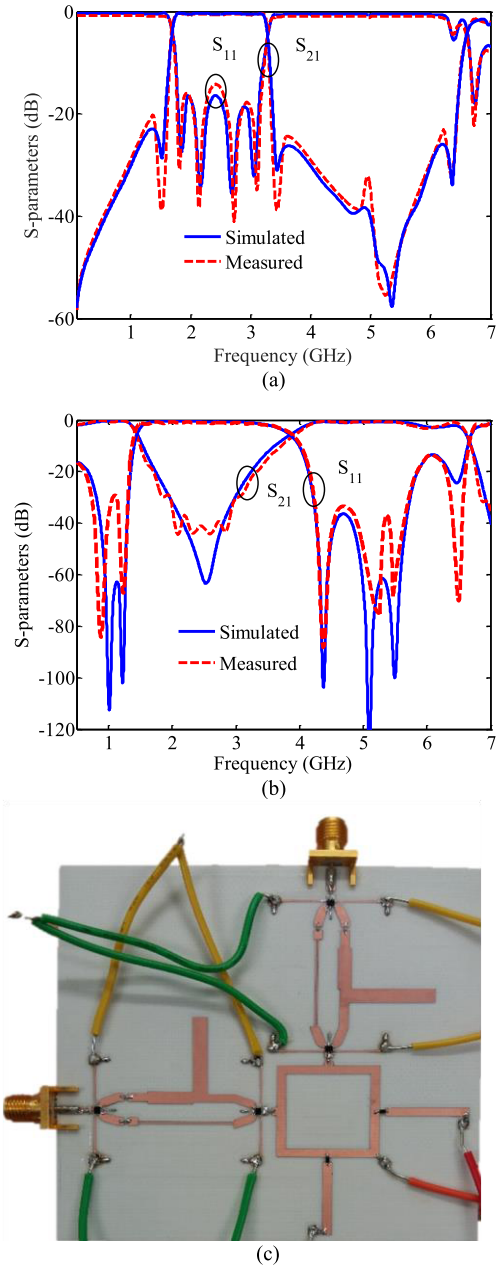

FIGURE 9. Simulated and measured S-parameters comparison (a) BPF state (PIN diodes ON, BPF feeding line section ON), (b) BSF state (PIN diodes OFF, BSF feeding line section ON), (c) photograph of the fabricated design.

350 and 385 dB/GHz respectively. The performance comparison between some reported BPFs topologies is shown in Table 2. It is observed that the proposed design provides a lower insertion loss and the highest ROR_{20dB} compared with the other reported designs and also has the ability to switch to a BSF state.

When the filter operates as a BSF it has measured stopband rejection of 40 dB along with 70% 20-dB fractional bandwidth. The measured attenuation rate at the lower side (passband to stopband transition) is 158 dB/GHz while the upper side attenuation rate is 43 dB/GHz. A comparison between

TABLE 2. Comparison with some previous BPF topologies.

Refs	S_{11} (dB)	S_{21} (dB)	FBW (%)	ROR (dB/GHz)
[10]	> 13	< 0.7	84	52/80
[11]	-	< 2.8	4.7	95/152
[33]	> 20	< 0.9	10	151/158
[34]	>10	< 1.5	30	37/62
[35]	> 28	<1.4	14.5	223/303
[38]	> 20	<1.0	30.2	52.6/109
This work	**> 15**	**< 0.86**	**65**	**350/385**

the proposed BSF with other reported BSF topologies is presented in Table 3. From table 3, it can be seen that the proposed BSF demonstrates the highest stopband rejection, with six transmission poles and also exhibits good skirt-band attenuation rates. The overall simulated and measured results for both filter states (BPF and BSF) are in very good agreement.

TABLE 3. Comparison with some previous BSF topologies.

Refs	20-dB FBW (%)	Passband RL (dB)	Lower and upper attenuation rates (dB/GHz)	TP	Stopband rejection (dB)
[2]	100	>10	61 & 38	2	-20
[3]	30	>13	15 & 56	2	-28
[4]	150	>10	425 & 212	6	-20
[5]	37.8	>10	35.4 & 35.4	3	-24
[6]	28	>10	63 & 63	5	-35
This work	**70**	**>15**	**158 & 43**	**6**	**-40**

VI. CONCLUSION

In this paper, a novel, and simple approach is proposed for the design of a reconfigurable bandpass (BPF)-to-bandstop (BSF) filter. The design is based on a microstrip square ring resonator where PIN diodes and SPDT switches are used to reconfigure the structure. The PIN diodes are implemented to either connect or disconnect the open-circuited $\lambda_g/4$ stubs on the ring resulting in bandpass or bandstop mode respectively. For superior filtering performances in both states, SPDT switches are used to either switch to BPF or BSF feeding line sections accordingly. The combination of the switches on both the ring resonator and the feeding line sections results in an excellent ROR_{20dB} and wide upper stopband in the bandpass mode, and excellent stopband rejection and good sharp stopband skirt in the bandstop mode. A detailed design analysis of the BPF-to-BSF transformation was also demonstrated through the use of even- and odd-mode analysis, which also explains the behavior of the resonances under weak coupling. For experimental validation, the reconfigurable filter was fabricated exhibiting both bandpass and bandstop responses with good agreement between simulations and measurements thus validating the proposed design. In the bandpass state, the filter had less than 0.86 dB of insertion loss for a 65% 3-dB bandwidth, whereas in the bandstop state, the filter

exhibited more than 40 dB stopband rejection. The proposed reconfigurable BPF to BSF with the novel selective feeding scheme integrated with SPDT switches demonstrates low insertion loss, high return loss and sharp roll-off response with high selectivity. The proposed filter topology can be used for frequency tunability in cognitive radio systems, for the isolation of the signals of interest or for the suppression of received interfering-signals.

ACKNOWLEDGMENT

The paper collaboration among NFC-Institute of Engineering & Fertilizer Research, Faisalabad, Pakistan; Frederick Research Center (FRC), Frederick University, Nicosia, Cyprus; Faculty of Computing and Informatics, University Malaysia Sabah, Kota Kinabalu, Malaysia; Department of Computer Science and Engineering, Hanyang University, Seoul, South Korea; and Research and Innovation Center of Excellence, University of Cyprus, Nicosia. The authors would like to thank Professor D. P. Kothari (Fellow, IEEE) and (Senior Editor, IEEE Access journal) for his valuable comments and suggestions on improving the article.

REFERENCES

[1] I. Shahid, D. N. Thalakotuna, D. K. Karmokar, and M. Heimlich, "Bandstop filter synthesis scheme for reactively loaded microstrip line based 1-D periodic structures," *IEEE Access*, vol. 8, pp. 155492–155505, 2020.

[2] M. Á. Sanchez-Soriano, G. Torregrosa-Penalva, and E. Bronchalo, "Compact wideband bandstop filter with four transmission zeros," *IEEE Microw. Wireless Compon. Lett.*, vol. 20, no. 6, pp. 313–315, Jun. 2010.

[3] A. Ebrahimi, W. Withayachumnankul, S. F. Al-Sarawi, and D. Abbott, "Compact second-order bandstop filter based on dual-mode complementary split-ring resonator," *IEEE Microw. Wireless Compon. Lett.*, vol. 26, no. 8, pp. 571–573, Aug. 2016.

[4] F.-C. Chen, R.-S. Li, J.-M. Qiu, and Q.-X. Chu, "Sharp-rejection wideband bandstop filter using stepped impedance resonators," *IEEE Trans. Compon., Package., Manuf. Technol.*, vol. 7, no. 3, pp. 444–449, Mar. 2017.

[5] H. Chen, D. Jiang, and X. Chen, "Wideband bandstop filter using hybrid microstrip/CPW-DGS with via-hole connection," *Electron. Lett.*, vol. 52, no. 17, pp. 1469–1470, Aug. 2016.

[6] T. Zhang, J. Bao, and Z. Cai, "Compact bandstop filter with high stopband attenuation," in *IEEE MTT-S Int. Microw. Symp. Dig.*, Honolulu, HI, USA, Jun. 2017, pp. 1916–1918.

[7] M. D. Hickle and D. Peroulis, "Theory and design of frequency-tunable absorptive bandstop filters," *IEEE Trans. Circuits Syst. I, Reg. Papers*, vol. 65, no. 6, pp. 1862–1874, Jun. 2018.

[8] K. B. Östman, M. Englund, O. Viitala, M. Kaltiokallio, K. Stadius, K. Koli, and J. Ryynanen, "Analysis and design of N-path filter offset tuning in a 0.7–2.7-GHz receiver front-end," *IEEE Trans. Circuits Syst. I, Reg. Papers*, vol. 62, no. 1, pp. 234–243, Jan. 2015.

[9] R. Gomez-Garcia, R. Loeches-Sanchez, D. Psychogiou, and D. Peroulis, "Single/multi-band wilkinson-type power dividers with embedded transversal filtering sections and application to channelized filters," *IEEE Trans. Circuits Syst. I, Reg. Papers*, vol. 62, no. 6, pp. 1518–1527, Jun. 2015.

[10] J. J. Sánchez-Martínez, E. Márquez-Segura, and S. Lucyszyn, "Design of compact wideband bandpass filters based on multiconductor transmission lines with interconnected alternate lines," *IEEE Microw. Wireless Compon. Lett.*, vol. 24, no. 7, pp. 454–456, Jul. 2014.

[11] S. Weng, K. Hsu, and W. Tu, "Microstrip bandpass single-pole quadruple-throw switch and independently switchable quadruplexer," *IET Microw., Antennas Propag.*, vol. 8, no. 4, pp. 244–254, Mar. 2014.

[12] T. Firmansyah, M. Alaydrus, Y. Wahyu, E. T. Rahardjo, and G. Wibisono, "A highly independent multiband bandpass filter using a multi-coupled line stub-SIR with folding structure," *IEEE Access*, vol. 8, pp. 83009–83026, 2020.

[13] G. Shen, W. Che, and Q. Xue, "Compact microwave and millimeter-wave bandpass filters using LTCC-based hybrid lumped and distributed resonators," *IEEE Access*, vol. 7, pp. 104797–104809, 2019.

[14] W. Xu, Y. Zhang, Y. Peng, J. Wang, L. Mu, B. Yu, and H. Zhang, "Tunable bandstop HMSIW filter with flexible center frequency and bandwidth using liquid crystal," *IEEE Access*, vol. 7, pp. 161308–161317, 2019.

[15] A. Quddious, M. A. B. Abbasi, A. Saghir, S. Arain, M. A. Antoniades, A. Polycarpou, P. Vryonides, and S. Nikolaou, "Dynamically reconfigurable SIR filter using rectenna and active booster," *IEEE Trans. Microw. Theory Techn.*, vol. 67, no. 4, pp. 1504–1515, Apr. 2019.

[16] S. Arain, P. Vryonides, A. Quddious, and S. Nikolaou, "Reconfigurable BPF with constant center frequency and wide tuning range of bandwidth," *IEEE Trans. Circuits Syst. II, Exp. Briefs*, vol. 67, no. 8, pp. 1374–1378, Aug. 2020.

[17] R. Allanic, D. Le Berre, Y. Quere, C. Quendo, D. Chouteau, V. Grimal, D. Valente, and J. Billoue, "A novel synthesis for bandwidth switchable bandpass filters using semi-conductor distributed doped areas," *IEEE Access*, vol. 8, pp. 122599–122609, 2020.

[18] S. Arain, P. Vryonides, M. A. B. Abbasi, A. Quddious, M. A. Antoniades, and S. Nikolaou, "Reconfigurable bandwidth bandpass filter with enhanced out-of-band rejection using π-section-loaded ring resonator," *IEEE Microw. Wireless Compon. Lett.*, vol. 28, no. 1, pp. 28–30, Jan. 2018.

[19] S. Arain, M. A. B. Abbasi, S. Nikolaou, and P. Vryonides, "A reconfiurable bandpass to bandstop filter using PIN diodes based on the square ring resonator," in *Proc. Prog. Electromagn. Res. Symp. (PIERS)*, Prague, Czech Republich, Jul. 2015.

[20] S. Arain, A. Quddious, A. Saghir, S. Nikolaou, and P. Vryonides, "Reconfigurable BPF with wide tuning bandwidth range using open-and short-ended stubs," in *Proc. 8th Int. Conf. Modern Circuits Syst. Technol. (MOCAST)*, Thessaloniki, Greece, May 2019, pp. 1–4.

[21] M. Jung and B.-W. Min, "A widely tunable compact bandpass filter based on a switched varactor-tuned resonator," *IEEE Access*, vol. 7, pp. 95178–95185, 2019.

[22] C. H. Kim and K. Chang, "Ring resonator bandpass filter with switchable bandwidth using stepped-impedance stubs," *IEEE Trans. Microw. Theory Techn.*, vol. 58, no. 12, pp. 3936–3944, Dec. 2010.

[23] P. Vryonides, S. Nikolaou, S. Kim, and M. M. Tentzeris, "Reconfigurable dual-mode band-pass filter with switchable bandwidth using PIN diodes," *Int. J. Microw. Wireless Technol.*, vol. 7, no. 6, pp. 655–660, Dec. 2015.

[24] L. Gao, T.-W. Lin, and G. M. Rebeiz, "Design of tunable multi-pole multi-zero bandpass filters and diplexer with high selectivity and isolation," *IEEE Trans. Circuits Syst. I, Reg. Papers*, vol. 66, no. 10, pp. 3831–3842, Oct. 2019.

[25] E. J. Naglich, J. Lee, D. Peroulis, and W. J. Chappell, "A tunable Bandpass-to-Bandstop reconfigurable filter with independent bandwidths and tunable response shape," *IEEE Trans. Microw. Theory Techn.*, vol. 58, no. 12, pp. 3770–3779, Dec. 2010.

[26] J. Lee, E. J. Naglich, H. H. Sigmarsson, D. Peroulis, and W. J. Chappell, "New bandstop filter circuit topology and its application to design of a bandstop-to-bandpass switchable filter," *IEEE Trans. Microw. Theory Techn.*, vol. 61, no. 3, pp. 1114–1123, Mar. 2013.

[27] Y.-H. Cho and G. M. Rebeiz, "Two- and four-pole tunable 0.7–1.1-GHz bandpass-to-bandstop filters with bandwidth control," *IEEE Trans. Microw. Theory Techn.*, vol. 62, no. 3, pp. 457–463, Mar. 2014.

[28] Y.-H. Cho and G. M. Rebeiz, "0.7–1.0-GHz reconfigurable bandpass-to-bandstop filter with selectable 2-and 4-pole responses," *IEEE Trans. Microw. Theory Techn.*, vol. 62, no. 11, pp. 2626–2632, Nov. 2014.

[29] Y.-M. Chen, S.-F. Chang, C.-Y. Chou, and K.-H. Liu, "A reconfigurable bandpass-bandstop filter based on varactor-loaded closed-ring resonators [Technical Committee]," *IEEE Microw. Mag.*, vol. 10, no. 1, pp. 138–140, Feb. 2009.

[30] M. Alqaisy, C. K. Chakrabraty, J. K. Ali, A. R. Alhawari, and T. Saeidi, "Switchable square ring bandpass to bandstop filter for ultra-wideband applications," *Int. J. Microw. Wireless Technol.*, vol. 9, no. 1, pp. 51–60, Feb. 2017.

[31] K. Song, W. Chen, S. R. Patience, Y. Chen, A. M. Iman, and Y. Fan, "Compact wide-frequency tunable filter with switchable bandpass and bandstop frequency response," *IEEE Access*, vol. 7, pp. 47503–47508, 2019.

[32] D. Psychogiou, R. Gomez-Garcia, and D. Peroulis, "Fully-reconfigurable bandpass/bandstop filters and their coupling-matrix representation," *IEEE Microw. Wireless Compon. Lett.*, vol. 26, no. 1, pp. 22–24, Jan. 2016.

[33] C.-S. Chen, J.-F. Wu, and Y.-S. Lin, "Compact single-pole-double-throw switchable bandpass filter based on multicoupled line," *IEEE Microw. Wireless Compon. Lett.*, vol. 24, no. 2, pp. 87–89, Feb. 2014.
[34] Z.-M. Tsai, Y.-S. Jiang, J. Lee, K.-Y. Lin, and H. Wang, "Analysis and design of bandpass single-pole–double-throw FET filter-integrated switches," *IEEE Trans. Microw. Theory Techn.*, vol. 55, no. 8, pp. 1601–1610, Aug. 2007.
[35] J. Xu, H. Wan, and Z.-Y. Chen, "Sharp skirt bandpass filter-integrated single-pole double-throw switch with absorptive OFF-state," *IEEE Trans. Microw. Theory Techn.*, vol. 67, no. 2, pp. 704–711, Feb. 2019.
[36] A. M. Zobilah, Z. Zakaria, and N. A. Shairi, "Selectable multiband isolation of single pole double throw switch using transmission line stub resonator for WiMAX and LTE applications," *IET Microw., Antennas Propag.*, vol. 11, no. 6, pp. 844–851, May 2017.
[37] J. Xu and Y. Zhu, "Tunable bandpass filter using a switched tunable diplexer technique," *IEEE Trans. Ind. Electron.*, vol. 64, no. 4, pp. 3118–3126, Apr. 2017.
[38] J. Xu, Q.-H. Cai, Z.-Y. Chen, and Y.-Q. Du, "Quasi-lumped-element filter-integrated single-pole double-throw switch," *IEEE Trans. Microw. Theory Techn.*, vol. 65, no. 11, pp. 4564–4571, Nov. 2017.
[39] L.-H. Hsieh and K. Chang, "Compact, low insertion-loss, sharp-rejection, and wide-band microstrip bandpass filters," *IEEE Trans. Microw. Theory Techn.*, vol. 51, no. 4, pp. 1241–1246, Apr. 2003.
[40] S. Sun, "A dual-band bandpass filter using a single dual-mode ring resonator," *IEEE Microw. Wireless Compon. Lett.*, vol. 21, no. 6, pp. 298–300, Jun. 2011.
[41] M. Matsuo, H. Yabuki, and M. Makimoto, "Dual-mode stepped-impedance ring resonator for bandpass filter applications," *IEEE Trans. Microw. Theory Techn.*, vol. 49, no. 7, pp. 1235–1240, Jul. 2001.
[42] S. Sun and L. Zhu, "Wideband microstrip ring resonator bandpass filters under multiple resonances," *IEEE Trans. Microw. Theory Techn.*, vol. 55, no. 10, pp. 2176–2192, Oct. 2007.
[43] I. Hunter, *Theory and Design Of Microwave Filters*. London, U.K: IEE, 2001.
[44] K. Chang, *Microwave Ring Circuits and Antennas*. New York, NY, USA: Wiley 1996.
[45] R. Zhang and L. Zhu, "Design of a wideband bandpass filter with composite short-and open-circuited stubs," *IEEE Microw. Wireless Compon. Lett.*, vol. 24, no. 2, pp. 96–98, Feb. 2014.
[46] *California Eastern Laboratories (CEL). High Power SPDT Switch*. [Online]. Available: http://www.cel.com/parts.do?command=load&idRootPart=2606

SALMAN ARAIN (Member, IEEE) received the B.E. degree in telecommunication engineering and the M.E. degree in telecommunication engineering and management from the Mehran University of Engineering and Technology, Pakistan, in 2012 and 2014, respectively, and the Ph.D. degree in electrical engineering (RF and microwave reconfigurable circuits) from Frederick University, Nicosia, Cyprus, in 2019, through the Erasmus Mundus INTACT Scholarship Program. He was awarded the six months Mobility Exchange Scholarship under Erasmus Mundus "Strong Ties" Program to complete his M.Eng. research at Frederick University, from 2013 to 2014. He is currently working as an Assistant Professor with the NFC-Institute of Engineering & Fertilizer Research, Faisalabad, Pakistan. His research interests include reconfigurable/switchable microwave devices mainly microwave filters and dividers/couplers, design of optical wireless communication networks, and spread spectrum communication systems. He is also a member of IET and Pakistan Engineering Council (PEC). He serves as a reviewer for various high quality journal publishers, such as IEEE, IET, Wiley, and Springer related to the field of microwave circuits and optical networks.

PHOTOS VRYONIDES (Member, IEEE) received the B.Eng., M.Phil., and Ph.D. degrees in electrical and electronic engineering from the University of Manchester Institute of Science and Technology (UMIST), U.K., in 1998, 1999, and 2002, respectively.

He is currently an Assistant Professor with Frederick University, where he is also a Senior Researcher with the Frederick Research Center (FRC). He is a member of the Antennas and Microwaves research group. He has authored or coauthored more than 50 papers in journals and peer-reviewed conferences. His research interests include mixers, LNAs, PAs, broadband amplifiers, millimeter-wave couplers, reconfigurable microwave filters, low phase noise oscillators, and millimeter-wave MMIC design and components. He is also a member of the Technical Chamber of Cyprus and has been a Cyprus Delegate in the Management Committee of COST IC0803 (RF/Microwave Communication Subsystems for Emerging Technologies) Action and CA18223 (Future Communications With Higher-Symmetric Engineered Artificial Materials). He serves as a Reviewer for the IEEE Microwave and Wireless Components Letters, IEEE Transactions on Circuits and Systems I: Regular Papers, IEEE Transactions on Circuits and Systems II: Express Briefs, and *IET Microwaves, Antennas & Propagation*.

KASHIF NISAR (Senior Member, IEEE) received the Ph.D. degree from the University of Technology PETRONAS, Malaysia. He did his Postdoctoral Research at the Auckland University of Technology, Auckland, New Zealand. Through his major in computer network and information technology, he has obtained solid training in research and development (R&D), writing funding proposal, journal publication, and as a Consultant. He is currently serving as an Associate Professor with the Faculty of Computing and Informatics, Universiti Malaysia Sabah, Kota Kinabalu, Malaysia. In 2014, he has served as a Guest Professor at Fernuniversität Hagen, Germany, funded by DAAD. He holds a number of visiting professor positions in well-known universities, such as McMaster University, Hamilton, ON, Canada; The University of Auckland, New Zealand; Hanyang University, South Korea; and Waseda University, Tokyo, Japan. He has published more than 160 research articles in many high impact journals and well reputed international conferences proceeding in the area of computer network. His research interests include future internet (FI), information centric network (ICN), content-centric networking (CCN), named data networking (NDN), software-defined networking (SDN), the Internet of Things (IoT), the Internet of Everything (IoE), the Industrial Internet of Things (IIoT), Fourth Industrial Revolution (IR 4.0), quantum networks, information security and privacy network/cyber security, digital forensics, applied cryptography, vehicular clouds, cloud and edge computing, and blockchain. He is currently working on future networks, IoT security, and API security, and he is also working closely with industries. He is a member of many professional organizations from academia and industry, including a Senior Member of IEEE (Founding IEEE Vice-Chair, Subsection), a member of ACM (ACM-SIGMOBILE, ISOC), Engineers Australia, IAENG, and Park Lab, and a Fellow of APAN and ITU. He is serving as an editorial board member for various journals, including IEEE Access, *IEEE Internet Initiative*, and *Internet Technology Letters* (Wiley), and serves as a reviewer for most of the IEEE Transactions, Springer, and Elsevier journals. He also serves as a technical program committee member of various conferences, such as IEEE GLOBECOM, IEEE R10 TENCOM, IEEE TrustCom, IEEE ICC, IEEE VTC, IEEE VNC, IEEE ICCVE, and ICCCN. He is also serving as a guest editor for more than a dozen of special issues in journals and magazines, such as IEEE, Elsevier, Springer, and Wiley.

ABDUL QUDDIOUS (Member, IEEE) received the B.S. degree in telecommunication engineering from GCUF, Faisalabad, Pakistan, in 2012, the M.S. degree in electrical engineering with majors in RF and microwaves from the Research Institute for Microwave and Millimeter-Wave Studies (RIMMS), NUST, Islamabad, Pakistan, in 2015, and the Ph.D. degree in electrical engineering (focusing on applied electromagnetics) from Frederick University, Nicosia, Cyprus, in 2019. From 2015 to 2016, he was a Lecturer with CIIT, Lahore, Pakistan. He is currently working with the KIOS Research and Innovation Center of Excellence, University of Cyprus, as a Postdoctoral Research Fellow and working on EU Horizon 2020 Future and Emerging Technologies (FET) Open project. His research interests include passive and active antennas, reconfigurable RF electronics, wireless power transfer, RFIDs, and implantable and wearable biomedical wireless sensors. He was a recipient of the Erasmus Mundus INTACT Doctoral Scholarship from European Union, in 2016. In 2019, he received an Honorary Gold Plaque for ''Academic Excellence'' from Frederick University, Cyprus.

SYMEON NIKOLAOU (Member, IEEE) received the B.S.E.C.E. degree in electrical and computer engineering from the National Technical University of Athens, in 2003, and the M.S.E.C.E. and Ph.D. degrees in electrical and computer engineering from the Georgia Institute of Technology, in 2005 and 2007, respectively.

He is currently an Associate Professor with Frederick University, Cyprus, where he is also a Senior Researcher with the Frederick Research Center. His research interests include the design of smart antennas, RFIDs/sensors, wearable and implantable antennas, and reconfigurable components for wireless transceivers.

Dr. Nikolaou is a member of the Technical Chamber of Cyprus and has been the Cyprus' Delegate in the Management Committee of COST IC0603 (ASSIST Antenna Systems & Sensors for Information Society Technology) Action and Substitute Delegate for Cyprus' Substitute Delegate in Management Committee of COST IC1102 (VISTA Action on Versatile, Integrated, and Signal-Aware Technologies for Antennas) Action, and is currently serving as the Cyprus' Delegate in the Management Committee of COST MiMED 1301 Accelerating the Technological, Clinical and Commercialization Progress in the Area of Medical Microwave Imaging. He serves as a Reviewer for the IEEE TRANSACTIONS ON ANTENNAS AND PROPAGATION, IEEE TRANSACTIONS ON ADVANCED PACKAGING, IEEE ANTENNAS AND WIRELESS PROPAGATION LETTERS, and *IET Letters*. He is currently an Associate Editor of *IET Microwaves Antennas & Propagation* and the International Journal on Antennas and Propagation (Open Access IJAP).